Hindawi
Advances in Materials Science and Engineering
Volume 2018, Article ID 8156812, 11 pages
https://doi.org/10.1155/2018/8156812

Research Article

Chemical, Mineralogical, and Refractory Characterization of Kaolin in the Regions of Huayacocotla-Alumbres, Mexico

L. M. Romero-Guerrero,[1] R. Moreno-Tovar,[1] A. Arenas-Flores,[1] Y. Marmolejo Santillán,[2] and F. Pérez-Moreno[1]

[1]*Área Académica de Ciencias de la Tierra y Materiales, Universidad Autónoma del Estado de Hidalgo, Carr. Pachuca-Tulancingo Km. 4.5 Col. Carboneras, 42184 Mineral de la Reforma, Hidalgo, Mexico*
[2]*Área Académica de Química, Universidad Autónoma del Estado de Hidalgo, Carr. Pachuca-Tulancingo Km. 4.5 Col. Carboneras, 42184 Mineral de la Reforma, Hidalgo, Mexico*

Correspondence should be addressed to F. Pérez-Moreno; fpmoreno@uaeh.edu.mx

Received 17 April 2018; Revised 18 August 2018; Accepted 30 September 2018; Published 1 November 2018

Academic Editor: Fernando Rubio-Marcos

In the present work, the chemical, mineralogical, refractory, and microstructural characterizations of kaolinites from the Huayacocotla-Alumbres region, which is between Veracruz and Hidalgo border, by X-ray diffraction (XRD), polarization optical microscopy (POM), scanning electron microscopy (SEM), refractoriness proof (pyrometric cone equivalent), and thermogravimetric analysis (TGA) were carried out. The analysis by POM showed that the kaolinization degree in this region is variable due to the presence of primary minerals, such as plagioclase, feldspar, and quartz. Additionally, hydrothermal alteration of the epithermal type was determined by oxidation of sulfides (pyrite and galena) and chlorite association. With the X-ray diffraction technique, andalusite and kaolinite were identified as the majority phases in Huayacocotla and quartz was identified as the majority phase in Alumbres. The minority phases, such as dickite, kaolinite, and cristobalite, were observed in both zones. The SEM technique was useful in the determination of the morphology of kaolinite and impurities of Na, Mg, K, and Fe of the complex clay illite-andalusite-dickite group. Thermogravimetric analysis was useful to discover the decomposition temperature and reveal the significant difference between 400 and 800°C, which showcases the greatest mass loss due to dehydration and carbonates decomposition. The mullite phase was detected at approximately 1000°C in the kaolin samples. The refractoriness tests were important to determine the stability temperature of kaolin, which is between 1300 and 1600°C. This stability temperature makes it feasible to use the kaolin as a refractory material for both low and high temperatures. The variables that affect the kaolin stability temperature were determined by principal components with the XLSTAT free program.

1. Introduction

Kaolin is a natural clay; it is an alteration product of feldspathic rocks whose main component is kaolinite [1]. Kaolin has wide application in industry due to its whiteness, inertness to chemical agents, electric insulator properties, mold ability, and ease of extrusion; also, it resists high temperatures, is nontoxic, and has high refractoriness. In Mexico, there are several kaolin deposits, and the most important ones are located in the States of Guanajuato, Hidalgo, and Veracruz [2].

Some characteristic problems of kaolin are the presence of minerals, such as iron oxide (hematite) and iron sulfides (pyrite), which act as coloring agents during the burning of ceramic pieces [3] and that the bending strength of ceramic tile is diminished when the pore size is reduced at a temperature higher than 1000°C [4]. Application techniques for clay purification that are used in pharmaceutical formulations are expensive because the clay used should have a high specific area, high adsorption capacity, high chemical inertness, and favorable rheological properties [5, 6].

Kaolin is an important raw material employed in ceramic manufacture; some kaolinite clay types have been used to prepare ceramics based on mullite because it has high-stability temperature, high refractoriness, high resistance to corrosive agents, and other desirable properties [7, 8]. The mineralogical compositions of clays are important aspects to evaluate since they directly influence the physical and mechanical qualities of fabricated ceramic products [7–10].

The kaolin exploitation has acquired great economic importance in recent years because its consumption has been increased in the manufacturing of products, such as paper, paints, inks, and plastics [1].

This study aims to assess the chemical, mineralogical, and refractory characteristics of kaolin from the Huayacocotla-Alumbres region in order to determine the material quality and propose possible application for it.

2. Materials and Methods

2.1. Study Area. The studied area, shown in Figure 1, is located in the east-central portion of the Mexican Republic, located to the northeast of Hidalgo state and northwest of Veracruz state. The area of Huayacocotla, Ver., is located between the coordinates 20°24′13″ N; 98°26′56″ W and 20°25′04″ N; 98°25′57″ W and the area of Alumbres, Hgo., is located between 20°40′18″ N; 98°41′15″ W and 20°40′22″ N; 98°41′10″ W, respectively.

The samples of kaolin were collected randomly on surface outcrop of mine that has been exploited in two zones that are shown in Figure 2.

The first zone is in Huayacocotla, Veracruz, localized among 20°24′13″ N; 98°26′56″ W and 20°25′04″ N; 98°25′57″ W, specifically in the mines of Rosa de Castilla, La Paloma, and Puerto Lobo; the access to this zone is leaving from Pachuca city in the direction to Tuxpan town by 130 Federal road and after passing the city of Tulancingo, 51 statal road must be taken to reach the mines in Agua Blanca, Huayacocotla, Ver.

The second zone is in Alumbres, Hidalgo, that is localized among 20°40′18″ N; 98°41′15″ W and 20°40′22″ N; 98°41′10″ W in Lote la Luz and Alumbres mines; the access to this zone is leaving from Pachuca city in the direction to Tampico town by the 105 Federal road and the towns Atotonilco el Grande, San Agustín Metzquititlan, and Zacualtipán must be traversed before reaching Alumbres, Hgo.

In the first zone, twenty-six samples were taken, and in the second, fifteen; these samples were chosen on the basis of their color, texture, and particle size, among other characteristics with an approximated weight of 1.5 kg each. They were placed in a plastic bag, sealed, and labeled with the location name, the date, and the georeferenced sampling point.

2.2. Analysis. The samples were dried at environmental temperature (30°C) without oven-drying over five days to remove the enough humidity to work with them. They were mixed and quartered to obtain a representative sample that was milled in an agate mortar to diminish the particle size; then, they were sieved on a set of 100, 200, 325, and 400 mesh to obtain subsamples with ranges of particle size 74–150; 45–74 and 38–45 μm is preferred for quantitative and qualitative analysis by spectrophotometric techniques [11, 12].

The chemical analysis was performed by triplicate; a 0.2 g clay sample of 38–45 μm of particle size was digested with an acid mixture of 4 ml of $HCl : HNO_3$ (3 : 1) and 7 ml of HF in a microwave oven, brand CEM mod. MARSLX. The sample temperature and pressure were raised up to 170°C and 170 psi in 25 min. These conditions were maintained for 15 min. Then, the samples were cooled, and 35 ml of H_3BO_3 (4%) was added to the containers to make a second digestion. The temperature and pressure were maintained at the same values as in the first digestion for 15 min; then, the volumetric flasks were filled with distilled water up to the 50 ml mark [13, 14]. The analysis was performed with an (ICP) spectrophotometer, PerkinElmer, model Optima 8300 XL, employing a multielemental-certified high-purity standard to determine the chemical composition of the principal elements of the oxide base in the laboratory of ICP and AA at the Autonomous University of Hidalgo State [15].

The detection limits for the analyzed samples were Mg (0.4), Mn (0.012), Na (0.04), Al (0.16), Ti (0.04), Ca (0.4), K (0.4), Fe (0.08), and Si (4) (mg L^{-1}).

The concentration conversion from mg·L^{-1}, provided by the ICP analysis, to the oxide percentage was carried out by using the periodic table to determine the molecular weight of the oxide compounds and employing the following equation:

$$\%O_m = \frac{C_L \times V_{af} \times F_d \times F_g}{W_s} \times \frac{1\ \text{g}}{1000\ \text{mg}} \times 100, \quad (1)$$

where O_m = metal oxide; C_L = concentration obtained by ICP (mg L^{-1}); V_{af} = flask volume (L); F_d = dilution factor; W_s = sample weight (g); and F_g = gravimetric factor = molecular weight of oxide (g)/atomic weight of metallic element (g).

The samples of 5 g with a particle size range of 74–150 μm were prepared for analysis by polarizing optical microscopy (POM), and the minimum quantity of the samples was placed in the sample holder (<1 g) with two resin drops in xylene and was covered with an object to obtain a uniform surface for subsequent identification with an Olympus Microscope model BX41 with the objectives 10X and 20X in transmitted light with parallel Nichols (PN) [16, 17].

The scanning electron microscopy (SEM) was performed employing a microscope JEOL, model JSM-6300, at 30 kV equipped with an EDS detector to take photomicrographs and to do chemical microanalysis. The samples of 0.2 g with a particle size range of 45–74 μm were placed in the metal sample holders using a double-side graphite adhesive tape; the samples were covered with a thin gold foil for 10 sec to achieve greater conductivity before their analysis.

The analysis by X-ray diffraction (XRD) was made on the clay samples of 5 g with a particle size range of 38–45 μm. The samples were placed in the sample holders to be analyzed in an INEL diffractometer, model EQUINOX 2000,

Figure 1: Kaoline area of Huayacocotla, Ver.,-Alumbres, Hgo., Mexico.

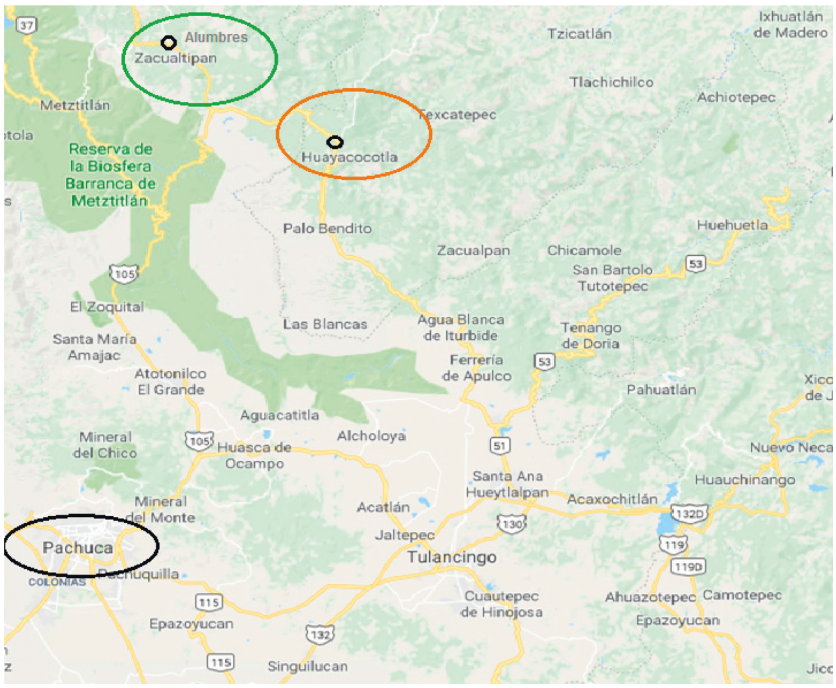

Figure 2: Access to the study zones of kaolin leaving from Pachuca, Hidalgo, Mexico.

with a simultaneous detector 2θ of 5–110° and Co Kα (1.789010 Å) cathode at 220 V for 30 min for the identification of the main mineral phases.

The refractoriness test was performed by employing a pyrometric cone equivalent (PCE) test, according to the C-24 ASTM standard [18]. The Arabian rubber and the kaolin with a particle size range of 38–45 μm were mixed to develop the pasta for manufacturing the test cones. The amount of Arabian rubber used was varied depending on the kaolin features. This pasta was placed in the cone mold and dried for a few minutes before removing it from its mold for its synthesis in the temperature range of 450°C up to 1600°C with a heating rate of 2.5°C min^{-1} in a Nabertherm furnace. Based on the SiO_2, Al_2O_3, and FeO content, five samples from Huayacocotla (H-RMC-1, H-RMC-4, H-RMC-5, H-RMC-15, and H-RMC-21), three samples from Alumbres (A-RMC-25, A-RMC-26, and A-RMC-29), and three Orton cones were used for this test.

The thermogravimetric analysis (TGA) was done with an equipment brand *Mettler Toledo* model *TGA/SDTA851^e*. Nine kaolin samples were selected at random from the two areas of the study; four of them corresponded to the Huayacocotla area (H-RMC-1, H-RMC-4, H-RMC-12, and H-RMC-21) and five to the Alumbres area (A-RMC-25,

A-RMC-26, A-RMC-29, A-RMC-38, and A-RMC-44). The samples of 3 ± 0.5 g with a particle size range of 74–150 μm were settled in 70 μL alumina crucibles and were heated from 50°C up to 1100°C with a heating rate of 10°C min^{-1} in a N_2 atmosphere with a 100 ml min^{-1} flow rate.

The statistical principal component analysis was performed using the XLSTAT Software. V. 18.07 [19] for determination of factors that affect kaolin stability temperature; this was done with the ICP and PCE data.

3. Results and Discussion

3.1. Chemical Analysis by ICP. The oxides' average percentage of principal elements are shown in Tables 1 and 2, and the minimum and maximum values and the standard deviation of the samples' total number in both zones are presented.

The values obtained for SiO_2 were heterogeneous in the two areas. In Huayacocotla, the minimum percentage is 21.7% and the maximum is 84.1% with the average of 65.3 ± 16.3%. In the Alumbres area, the minimum value is 41.6% and the maximum is 87.8%, with an average of 69.3 ± 14.6%.

The Al_2O_3 concentration in the Huayacocotla samples is heterogeneous, with a minimum value of 6.3%, a maximum value of 30.7%, and an average of 19.3 ± 6.6%. In the Alumbres area, the behavior is similar, with a minimum value of 7.8%, a maximum value of 36.0%, and an average of 19.3 ± 7.8%.

Additionally, FeO is present in the heterogeneous concentration in both areas. In Huayacocotla, the minimum value is 0.1% and the maximum value is 6.2%. In Alumbres, the values are 0.1% and 19.0%, the minimum and maximum, respectively. The last area shows that the FeO percentage is higher than that in the first area; this is also reflected by the material coloration.

TiO_2 has been evaluated, and it has a relatively low concentration in the two areas; Huayacocotla presented 0.1% and 0.7% as the minimum and maximum values, respectively, and 0.4 ± 0.4% as the average. Alumbres presented 0.1% and 1.3% as the minimum and maximum values, respectively, and 0.5 ± 0.4% as the average. TiO_2 can be associated with presence of rutile, which is the most common mineral of titanium dioxide; however, polymorphs rarely include brookite and anatase, both form unique and distinctive crystals on the earth, and this is typical in felsic rocks [20].

The CaO concentration is heterogeneous, the minimum value recorded in Huayacocotla is <0.1%, the maximum value is 0.6%, and the average value is 0.2 ± 0.2%. Alumbres has the minimum value of 0.1%, maximum value of 0.4%, and the average value of 0.2 ± 0.1%.

The Na_2O concentration in Huayacocotla is higher than that in Alumbres. The first has a minimum value of 0.1%, a maximum value of 1.6%, and an average value of 0.6 ± 0.5%, while the Alumbres region has a minimum value of 0.1%, a maximum value of 0.4%, and an average value of 0.2 ± 0.1%.

Concentrations of CaO and Na_2O in both areas can mean reflection of altered calco-sodium plagioclase that is represented by clay in this region. Additionally, the percentages of MgO and MnO in the same areas are <0.01%; thus, these results are omitted from Tables 1 and 2. The oxide percentages of elements in the kaolin samples were similar to that in potassium feldspar (K-Feld) reported by Walsh and Howie [15].

3.2. Polarizing Optical Microscopy (POM). The analysis by POM allowed the observance of clay samples from Huayacocotla with a habit crystalline acicular that is weakly associated with minerals of high relief. Some of the clay samples present intergrowths with opaque minerals; these samples are appreciable crystalline forms of K-Feld, quartz, and plagioclase with iron oxides development on their cleavage, as shown in Figure 3(a).

Figure 3(b) shows minerals as high-relief impurities with crystalline habits from anhedral to subhedral; these are represented by quartz, plagioclase, and K-Feld. The last two minerals are associated with opaque mineral intergrowths, and their cleavage is also observed with some spheroidal minerals, which possibly correspond to chlorite.

Kaolin samples from Alumbres contain significant amounts of opaque minerals with a crystalline cubic system, such as pyrite, some coarse grits intergrowth with iron oxides on strongly oxidized clay, and high developments of metallic pyrite minerals, as is shown in Figure 4(a); therefore, this represents a hydrothermal alteration area [21].

Sometimes, pollution is observed by high-relief minerals associated with plagioclase, quartz, and opaque minerals; all of these minerals are derived from protolithic (rhyolite) that presents three clays types: acicular, not acicular, and granular with a high hardness from silica. The clays also present coloration due to a chlorite presence, as shown in Figure 4(b).

The POM confirms the high content of SiO2, FeS, and FeO in certain samples from Alumbres and Huayacocotla, and the different minerals are associated with the kaolin. Employing this technique is important for the determination and contrasting of the interferences present in each area.

3.3. Scanning Electron Microscopy (SEM). The kaolin morphologies are similar in both areas, but different mineral species are observed in the Alumbres samples. In Figure 5, there are particles with crystalline habit of the subhedral to euhedral type with well-defined plans; these could correspond to kaolinite (Figure 5(a)), dickite (Figure 5(b)), and illite (Figure 5(c)) in aggregate form.

Morphological analysis by SEM was performed on the Huayacocotla samples, allowing the identification of kaolinite in H-RMC-2 and H-RMC-3 and dickite in H-RMC-6, H-RMC-12, and H-RMC-16. In the Alumbres samples, illite in A-RMC-25, kaolinite in A-RMC-31, A-RMC-38, and A-RMC-39, and dickite in A-RMC-45 were identified. The elemental semiquantitative analyses performed on these samples are shown in Table 3; they were also identified by SEM-EDS and showed the same characteristics that were mentioned previously.

Table 1: Oxide percentage of kaolin majority elements of Huayacocotla.

	Huayacocotla zone, % oxide (SD)							
Sample	SiO_2	Al_2O_3	FeO (T)	TiO_2	CaO	K_2O	Na_2O	SO_2
H-RMC-1	36.1 (1.5)	19.2 (2.5)	0.2 (0.1)	0.6 (0.1)	0.2 (0.1)	1.8 (0.3)	1.4 (0.3)	0.6 (0.1)
H-RMC-2	76.8 (2.3)	15.3 (1.3)	0.4 (0.1)	0.2 (0.1)	0.6 (0.0)	0.5 (0.2)	1.5 (0.6)	0.3 (0.0)
H-RMC-3	66.9 (2.2)	19.5 (1.9)	0.1 (0.1)	0.2 (0.0)	0.4 (0.0)	1.1 (0.2)	1.5 (0.4)	0.6 (0.1)
H-RMC-4	47.3 (2.0)	29.4 (1.4)	6.2 (0.4)	0.9 (0.1)	0.6 (0.0)	0.9 (0.1)	1.6 (0.4)	0.7 (0.2)
H-RMC-5	51.4 (2.2)	30.7 (0.9)	0.2 (0.1)	1.7 (0.3)	0.2 (0.0)	0.1 (0.1)	0.4 (0.2)	0.6 (0.1)
H-RMC-6	72.1 (2.1)	17.7 (1.0)	0.3 (0.1)	0.3 (0.0)	0.1 (0.1)	0.2 (0.1)	0.7 (0.4)	0.2 (0.0)
H-RMC-7	77.1 (1.2)	6.3 (1.7)	0.1 (0.1)	0.3 (0.1)	0.1 (0.0)	1.3 (0.2)	0.4 (0.1)	0.3 (0.1)
H-RMC-8	73.5 (1.3)	15.1 (1.6)	0.1 (0.1)	0.5 (0.0)	0.2 (0.0)	0.4 (0.4)	0.4 (0.3)	0.2 (0.0)
H-RMC-9	66.7 (1.4)	19.6 (1.2)	0.4 (0.2)	0.9 (0.1)	0.1 (0.1)	0.1 (0.1)	0.3 (0.1)	0.4 (0.1)
H-RMC-11	44.3 (1.2)	29.9 (1.3)	0.5 (0.1)	1.3 (0.3)	0.2 (0.0)	1.2 (0.2)	0.6 (0.1)	0.3 (0.1)
H-RMC-12	36.6 (1.4)	24.7 (0.9)	0.3 (0.2)	0.3 (0.1)	0.2 (0.0)	1.5 (0.1)	1.6 (0.4)	1.0 (0.4)
H-RMC-14	72.0 (1.4)	16.3 (0.9)	0.1 (0.0)	0.2 (0.1)	0.6 (0.1)	0.4 (0.2)	1.3 (0.2)	0.6 (0.2)
H-RMC-15	74.3 (1.7)	16.5 (1.2)	0.2 (0.0)	0.3 (0.2)	0.3 (0.1)	0.3 (0.3)	0.3 (0.2)	0.4 (0.1)
H-RMC-16	84.1 (1.6)	12.3 (1.0)	0.1 (0.1)	0.1 (0.0)	0.1 (0.0)	0.1 (0.1)	0.2 (0.1)	1.1 (0.4)
H-RMC-17	60.6 (1.7)	22.1 (1.2)	0.1 (0.0)	0.1 (0.0)	0.1 (0.0)	1.3 (0.1)	0.6 (0.2)	2.1 (0.6)
H-RMC-18	73.6 (1.1)	19.0 (1.4)	0.1 (0.0)	0.3 (0.1)	0.1 (0.0)	0.5 (0.2)	0.4 (0.2)	1.9 (0.5)
H-RMC-19	82.6 (1.7)	11.7 (1.3)	0.1 (0.0)	0.1 (0.0)	0.4 (0.0)	0.2 (0.1)	0.1 (0.1)	0.1 (0.0)
H-RMC-20	78.3 (1.9)	16.7 (1.1)	0.1 (0.0)	0.2 (0.1)	0.1 (0.0)	0.6 (0.2)	0.2 (0.1)	0.2 (0.0)
H-RMC-21	80.0 (1.6)	16.7 (1.9)	0.1 (0.1)	0.2 (0.0)	0.1 (0.1)	0.2 (0.1)	0.2 (0.1)	0.3 (0.1)
H-RMC-22	79.8 (1.2)	14.7 (1.1)	0.2 (0.1)	0.3 (0.2)	0.1 (0.0)	0.1 (0.1)	0.1 (0.1)	0.7 (0.2)
H-RMC-23	78.4 (1.8)	16.8 (1.4)	0.2 (0.0)	0.2 (0.1)	<0.1	0.2 (0.1)	0.1 (0.1)	0.9 (0.3)
H-RMC-32	21.7 (2.5)	27.9 (2.1)	0.1 (0.1)	0.2 (0.1)	<0.1	2.1 (0.1)	0.6 (0.1)	0.3 (0.0)
H-RMC-33	71.3 (1.7)	11.0 (1.3)	0.1 (0.0)	0.2 (0.0)	0.1 (0.1)	1.5 (0.1)	0.3 (0.1)	0.3 (0.0)
H-RMC-35	65.0 (1.4)	26.9 (1.4)	0.1 (0.1)	0.7 (0.2)	0.1 (0.1)	0.5 (0.2)	0.4 (0.3)	0.3 (0.0)
H-RMC-36	60.5 (1.7)	30.7 (1.3)	0.2 (0.1)	0.9 (0.1)	0.1 (0.1)	0.1 (0.1)	0.5 (0.3)	0.4 (0.1)
H-RMC-37	66.3 (1.9)	15.7 (1.7)	0.1 (0.0)	0.3 (0.1)	<0.1	1.4 (0.2)	0.5 (0.1)	0.4 (0.1)
Mean	65.3 (16.3)	19.3 (6.6)	0.4 (1.2)	0.4 (0.4)	0.2 (0.2)	0.7 (0.6)	0.6 (0.5)	0.6 (0.5)

FeO (T) was determined as total iron.

Table 2: Oxide percentage of kaolin majority elements of Alumbres.

	Alumbres zone, oxides % (SD)							
Sample	SiO_2	Al_2O_3	FeO (T)	TiO_2	CaO	K_2O	Na_2O	SO_2
A-RMC-25	60.9 (1.5)	13.6 (1.4)	14.0 (0.7)	0.4 (0.1)	0.1 (0.1)	1.6 (0.29)	0.1 (0.1)	0.5 (0.2)
A-RMC-26	41.6 (1.9)	16.3 (1.3)	19.0 (0.4)	1.2 (0.1)	0.2 (0.3)	1.5 (0.2)	0.1 (0.0)	0.4 (0.2)
A-RMC-27	68.9 (1.8)	16.6 (1.5)	0.5 (0.5)	0.2 (0.0)	0.1 (0.1)	1.5 (0.1)	0.4 (0.1)	0.3 (0.1)
A-RMC-28	87.7 (2.5)	11.5 (1.6)	0.2 (0.1)	0.3 (0.1)	0.1 (0.1)	0.7 (0.1)	0.4 (0.2)	0.3 (0.1)
A-RMC-29	60.6 (1.8)	36.0 (1.3)	0.3 (0.0)	1.3 (0.3)	0.1 (0.1)	0.1 (0.2)	0.4 (0.1)	0.3 (0.1)
A-RMC-30	73.6 (1.9)	21.4 (1.5)	0.2 (0.1)	0.3 (0.0)	0.2 (0.2)	0.6 (0.1)	0.2 (0.0)	0.6 (0.2)
A-RMC-31	78.5 (1.5)	21.4 (1.8)	0.1 (0.0)	0.2 (0.0)	0.2 (0.2)	0.1 (0.1)	0.2 (0.0)	0.1 (0.0)
A-RMC-38	87.8 (2.1)	7.8 (1.9)	1.5 (0.2)	0.4 (0.1)	0.1 (0.1)	0.2 (0.2)	0.1 (0.0)	0.4 (0.1)
A-RMC-39	51.2 (1.8)	31.3 (1.3)	6.3 (0.2)	1.3 (0.3)	0.4 (0.6)	0.1 (0.0)	0.3 (0.0)	0.4 (0.1)
A-RMC-40	78.7 (2.1)	18.6 (1.5)	0.2 (0.2)	0.3 (0.2)	0.4 (0.6)	0.7 (0.1)	0.1 (0.0)	0.4 (0.2)
A-RMC-41	58.6 (1.6)	22.6 (1.2)	0.1 (0.1)	0.2 (0.0)	0.4 (0.5)	1.7 (0.2)	0.4 (0.0)	0.4 (0.1)
A-RMC-42	83.4 (2.1)	13.4 (1.7)	0.1 (0.0)	0.4 (0.2)	0.1 (0.1)	1.2 (0.4)	0.2 (0.0)	0.4 (0.2)
A-RMC-43	84.5 (1.8)	10.7 (1.9)	0.1 (0.1)	0.1 (0.0)	0.3 (0.4)	0.8 (0.2)	0.2 (0.0)	0.4 (0.2)
A-RMC-44	51.3 (1.8)	26.4 (1.3)	0.1 (0.1)	0.2 (0.1)	0.4 (0.6)	1.5 (0.2)	0.1 (0.0)	0.4 (0.2)
A-RMC-45	72.5 (1.7)	22.4 (1.5)	0.1 (0.1)	0.2 (0.2)	0.4 (0.5)	0.4 (0.6)	0.1 (0.0)	0.4 (0.1)
Mean	69.3 (14.6)	19.3 (7.8)	2.9 (5.8)	0.5 (0.4)	0.2 (0.1)	0.8 (0.6)	0.2 (0.1)	0.4 (0.1)

FeO (T) was determined as total iron.

3.4. X-Ray Diffraction (XRD). The representative samples of kaolin in the two zones were selected for their high and low content of SiO2 to be analyzed by XRD, and they were evaluated with the Software Match V.3 and cards PDF-02 of the diffraction patterns. The major crystalline phases observed in Huayacocotla samples were andalusite (Al_2SiO_5), kaolinite ($Al_2Si_2O_5(OH)_4$), and cristobalite (SiO_2), and the major crystalline phases in Alumbres were quartz (SiO_2) and andalusite. The minority crystalline phases were quartz and kaolinite in Huayacocotla and pyrite (FeS_2) and dickite ($Al_2Si_2O_5(OH)_4$) in Alumbres. Finally, quartz, illite, sillimanite (Al_2SiO_5), and magnetite (Fe_3O_4) were identified as vestige mineral phases in both zones, as shown in Table 4.

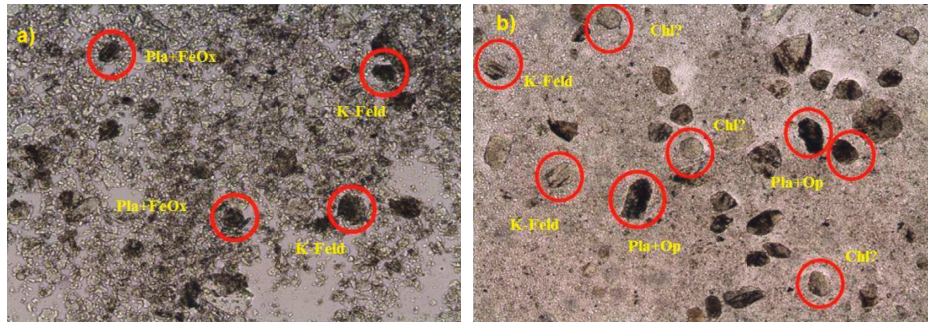

Figure 3: Polarization optical microscopy of Huayacocotla kaolin. (a) K-Feld and plagioclase with iron oxides (Pla + FeOx). (b) Spheroidal minerals, possible chlorite (Chl), plagioclase with opaque minerals (Pla + Op), K-Feld. Conditions: parallel Nichols, objective 10X, and 0.98 mm photography horizontal field.

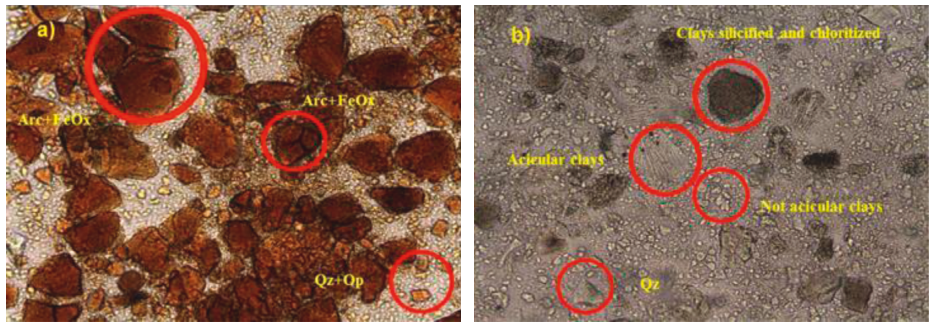

Figure 4: Minerals present in kaolin. (a) Minerals with high oxidation, clay with iron oxide (Arc + FeOx). (b) Minerals acicular, not acicular, and granular with possible chlorite (Chl) content. POM with parallel Nichols, objective 10X, and 0.98 mm photography horizontal field.

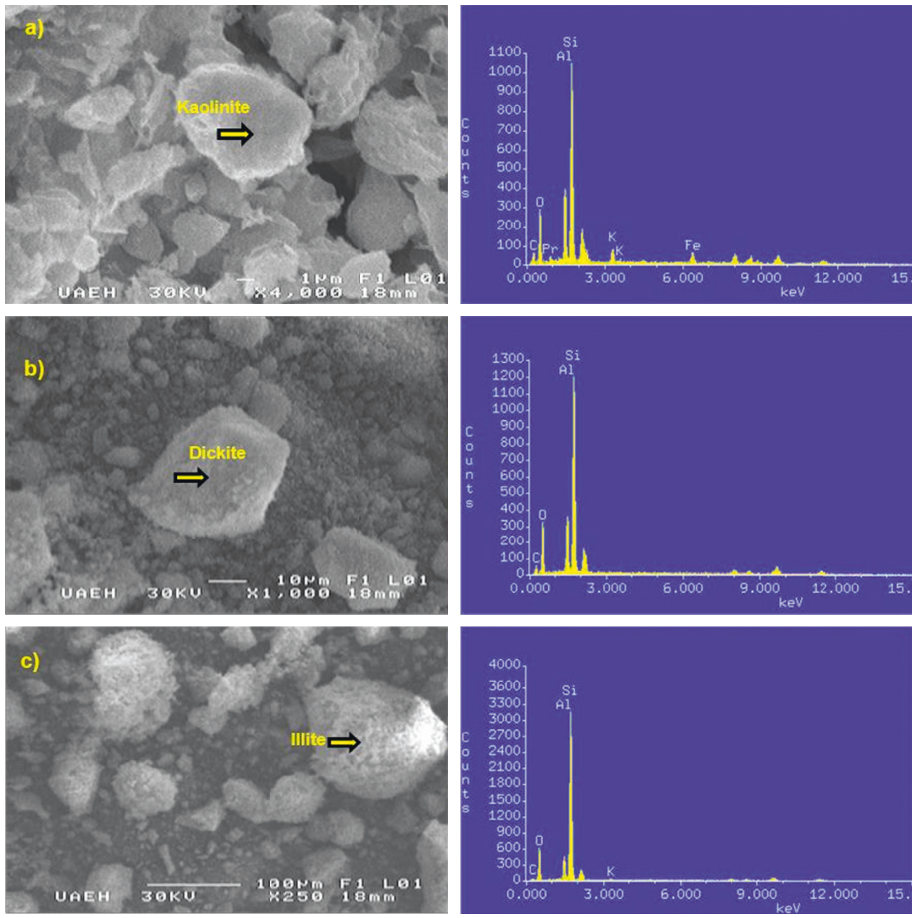

Figure 5: Kaolin minerals determined by SEM and EDS. (a) Kaolinite in H-RMC-2. (b) Dickite in H-RMC-16. (c) Illite in A-RMC-25.

Table 3: Semiquantitative analysis of the kaolin samples by SEM in percentage weight (SD).

Compounds	H-RMC-2	H-RMC-3	H-RMC-6	H-RMC-16	A-RMC-25	A-RMC-31	A-RMC-38	A-RMC-39
SiO_2	69.8 (4.6)	66.0 (5.2)	76.4 (5.0)	80.8 (5.4)	88.7 (7.4)	81.1 (6.8)	76.9 (4.6)	54.9 (3.6)
Al_2O_3	21.2 (1.4)	31.7 (2.8)	21.7 (2.4)	18.7 (2.4)	10.0 (2.4)	18.0 (3.6)	22.1 (3.4)	41.6 (4.6)
Na_2O	0.1 (0.1)	0.1 (0.1)	0.1 (0.1)	0.1 (0.1)	0.1 (0.1)	0.4 (0.1)	0.1 (0.1)	0.1 (0.1)
MgO	1.0 (0.4)	0.2 (0.1)	0.1 (0.1)	0.1 (0.1)	0.3 (0.1)	0.1 (0.1)	0.2 (0.1)	0.2 (0.1)
K_2O	2.7 (0.8)	1.1 (0.6)	0.1 (0.1)	0.1 (0.1)	0.2 (0.1)	0.2 (0.1)	0.1 (0.1)	0.1 (0.1)
CaO	0.1 (0.1)	0.1 (0.1)	0.1 (0.1)	0.1 (0.1)	0.1 (0.1)	0.1 (0.1)	0.1 (0.1)	0.1 (0.1)
FeO	4.5 (1.4)	0.4 (0.1)	0.1 (0.1)	0.1 (0.1)	0.4 (0.1)	0.1 (0.1)	0.4 (0.1)	1.3 (0.4)
TiO_2	0.7 (0.2)	0.5 (0.1)	1.6 (0.4)	0.2 (0.1)	0.2 (0.1)	0.2 (0.1)	0.2 (0.1)	1.7 (0.4)

The lower diffractogram of Figure 6 shows the main phases of the kaolin sample H-RMC-21 without heat treatment, which shows the kaolinite ($Al_2Si_2O_5(OH)_4$ with PDF 00-003-0052) and andalusite (Al_2SiO_5, PDF 00-039-0376). The XRD analysis was performed on kaolin H-RMC-21 that was sintered at 1450°C, and the phases that are observed are *ß*-cristobalite (SiO_2, PDF 01-082-1407) and pseudomullite ($3(Al_2O_3.SiO_2)$, PDF 00-002-1160), as seen in the upper part of Figure 7. The transformation of the phases occurs as the temperature increases, and the silica is transformed into its different polymorphic forms, such as low quartz (573°C), high quartz (867°C), tridymite (>1400°C), and cristobalite (>1450°C). Simultaneously, there is a reaction of alumina with silica that originates presence of pseudomullite. It is not possible to observe the mullite phase formation due to the higher alumina content and the formation of eutectic, which favors the dissolution of alumina in a transitional phase of liquid silica above 1500°C [22, 23]. Diffractograms of kaolin treated at temperatures up to 1600°C have the same phases.

3.5. Refractoriness Test (PCE). The pyrometric cone equivalent (PCE) test for the kaolin samples from Huayacocotla and Alumbres can help us to determine the stability temperature (T_{St}), the softening (T_{So}), and/or vitrification (T_V) of the kaolin.

As the temperature was increased, the samples acquired a reddish tone that varied according to the iron content of the samples; however, after 1200°C, the test cones recovered their white color, except those whose iron content was higher than 5%.

According to the temperature employed in the pyrometric tests, it was possible to observe stability temperatures below 1300°C and up to 1600°C and softening temperatures and vitrification from approximately 1600°C and above, as is shown in Figure 7.

Principal component analysis is useful in the determination of the parameters that influence the thermal stability of kaolin for which the PCE values (Figure 2) and oxides composition data (Tables 1 and 2) are used to standardize each variable to the mean zero, and the unit variance is used to make all variables have the same weight in the analysis to obtain the Pearson correlation (Table 5).

It is observed in Table 5 that the stability temperature of kaolin varies directly with the content of SiO_2 and inversely with the content of K_2O and that the contents of Al_2O_3, FeO, and CaO correlate directly with contents of TiO_2, K_2O, and Na_2O, respectively.

Table 4: Analysis of principal and secondary phases of the kaolin samples at Huayacocotla and Alumbres by XRD.

Sample	Principal phase (>50%)	Secondary phase (10–40%)	Trace (<5%)
	Huayacocotla		
H-RMC-4	An	Kln	—
H-RMC-9	Cr	Kln	Mag
H-RMC-14	Cr	Kln	Qz
H-RMC-21	An	Kln	Mag
H-RMC-32	An	Qz	—
H-RMC-35	Kln	Qz	—
	Alumbres		
A-RMC-25	Qz	Py	Ill
A-RMC-26	Qz	Py	Kln, Ill
A-RMC-40	An	Dck	Cr, Ill, Sil
A-RMC-45	An	Dck	Qz,

An = andalusite, Cr = cristobalite, Qz = quartz, Kln = kaolinite, Dck = dickite, Py = pyrite, Mag = magnetite, Ill = illite, Sil = sillimanite.

The principal component analyses of kaolin from the Huayacocotla-Alumbres region are shown in Figure 8, where components F1 and F2 are the main weights. In this figure, the stability temperature correlates positively with F1 and F2 components, negatively with K_2O and FeO; the stability temperature does not correlate with Al_2O_3 or SiO_2 but correlates negatively with the content of Na_2O, CaO, and SO_2.

The softening temperature of kaolin is due to presence of K_2O, Na_2O, CaO, FeO, and SO_2. The vitrification temperature depends on the content of SiO_2, whereas high stability depends on the Al_2O_3 content.

3.6. Thermogravimetric Analysis (TGA). The TGA obtained for the kaolin samples is shown in Figure 9; the samples present characteristic sigmoidal curves and significant loss of mass, which starts at 400°C and ends near 850°C.

Working conditions are as follows: thermogravimetric analyzer, Mettler Toledo, Mod. TGA/SDTA851[e], with a range from 50 to 1100°C with a heating rate of 10°C min^{-1}, a N_2 atmosphere, and a flow rate of 100 ml·min^{-1}.

It was possible to observe desorption of surface water in the samples H-RMC-4, A-RMC-25, and A-RMC-26 from 50 to 100°C.

The samples started their decomposition between 456°C and 576°C. The hydroxyl groups were removed from the crystal network of ore, and kaolinite was transformed to

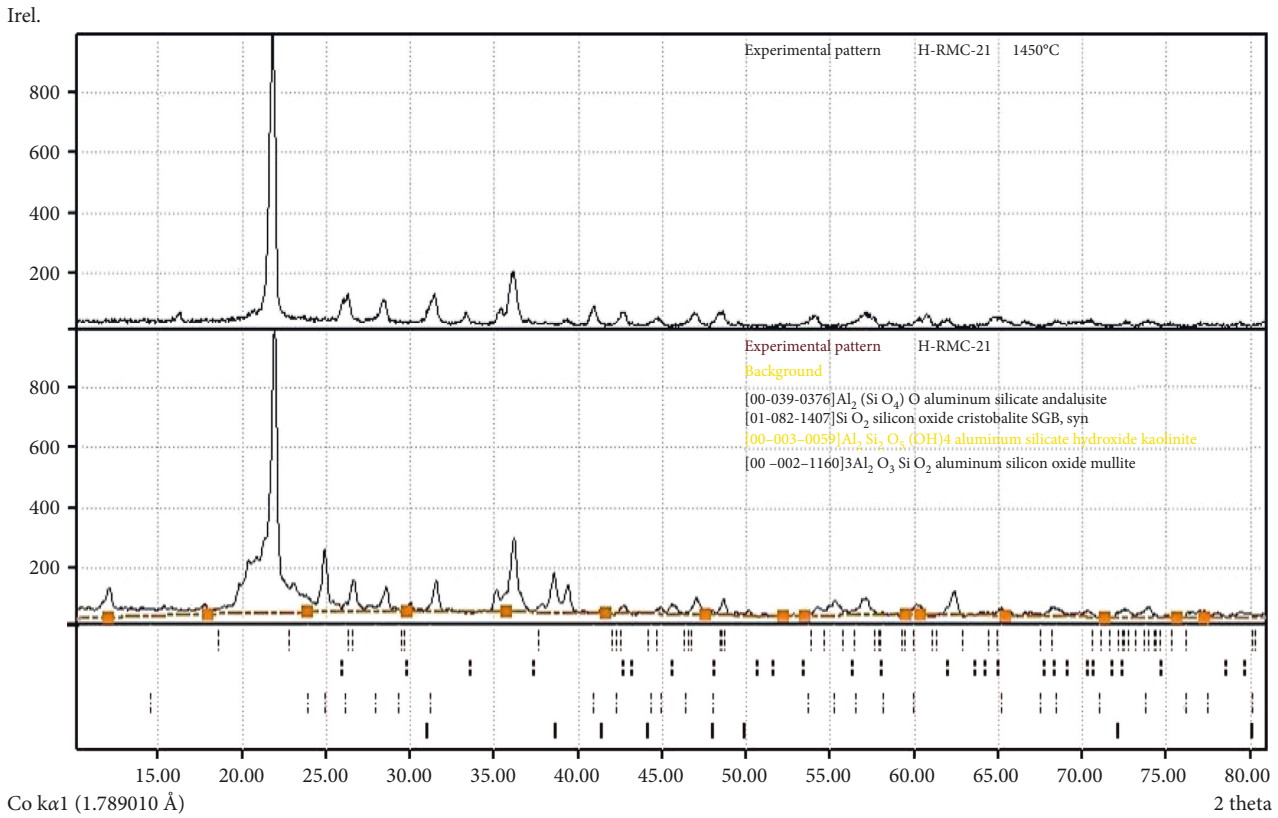

Figure 6: Diffractogram of the sample H-RMC-21 with and without thermal treatment.

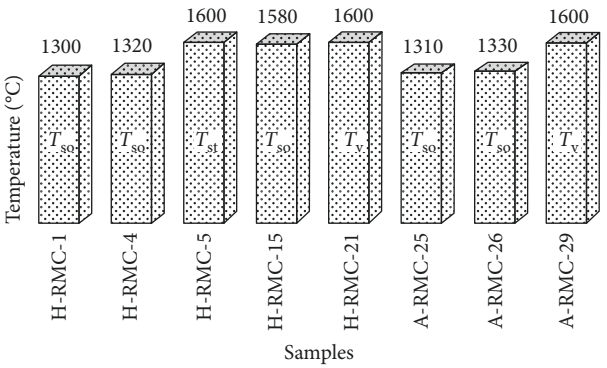

Figure 7: Kaolin thermal treatment of Huayacocotla, Ver., and Alumbres, Hgo., samples. Stability temperature (T_{St}), softening (T_{So}), and/or vitrification (T_V) of the kaolin.

metakaolinite with the water loss of all samples; this derivative is low quartz according to the SDTA data of A-RMC-44 of Figure 9 by equilibrium 2 [6, 24–27]:

$$\underset{\text{Kaolinite}}{Si_2Al_2O_5(OH)_4} \xrightarrow{456-576^{\circ}C} \underset{\text{Metakaolinite}}{Al_2O_3 2SiO_2} + 2H_2O \quad (2)$$

The samples H-RMC-1, H-RMC-12, H-RMC-21, A-RMC-29, and A-RMC-38 present low mass loss, which is characteristic of well-crystallized kaolinite. The H-RMC-4 samples, A-RMC-25, A-RMC-26, and A-RMC-44 exhibit a high mass loss. This behavior can be attributed to two factors. The first is water elimination retained between blades of ore, and the second is determined by reorganization of other present minerals and silica polymorphs, such as low and high quartz and tridymite.

In the heating stage, which starts at 739°C and continues up to 850°C, there is mass loss in samples that is mainly attributable to the impurities present in kaolin that contains carbonates, etc. Once these dehydration processes and decomposition are completed, the samples behave stably up to approximately 950°C.

The kaolin samples having low losses of mass at temperatures under 950°C is indicative of high purity. So as seen in Figure 10, the samples H-RMC-21, A-RMC-29, and A-RMC-38 have a high purity, while the samples H-RMC-4, A-RMC-26, and A-RMC-44 are less pure.

The TGA data of A-RMC sample were converted to SDTA, and at approximately 1000°C, the formation of mullite can also be observed, as is shown in Figure 9, according to the equilibrium 3:

$$\underset{\text{Metakaolinite}}{2(Al_2O_3 2SiO_2)} \xrightarrow{989-1009^{\circ}C} \underset{\text{Mullite}}{Al_4Si_2O_{10}} + \underset{\beta-\text{cristobalite}}{2SiO_2} \quad (3)$$

4. Conclusions

The principal mineral phases identified in the Huayacocotla samples are cristobalite, andalusite, and kaolinite; and the

Table 5: Pearson correlation of kaolin from Huayacocotla Ver. and Alumbres Hgo.

Variables	SiO_2	Al_2O_3	FeO	TiO_2	CaO	K_2O	Na_2O	SO_2	T_{St}
SiO_2	**1**	−0.191	−0.344	−0.519	−0.284	−0.643	−0.546	−0.637	0.620
Al_2O_3	−0.191	**1**	−0.427	**0.727**	0.236	−0.530	0.331	0.172	0.421
FeO	−0.344	−0.427	**1**	0.062	0.006	0.634	−0.284	0.036	−0.650
TiO_2	−0.519	**0.727**	0.062	**1**	0.056	−0.219	0.026	0.223	0.235
CaO	−0.284	0.236	0.006	0.056	**1**	0.044	0.704	0.661	−0.339
K_2O	−0.643	−0.530	0.634	−0.219	0.044	**1**	0.272	0.385	**−0.940**
Na_2O	−0.546	0.331	−0.284	0.026	0.704	0.272	**1**	**0.733**	−0.430
SO_2	−0.637	0.172	0.036	0.223	0.661	0.385	**0.733**	**1**	−0.487
St_T (°C)	0.620	0.421	−0.650	0.235	−0.339	**−0.940**	−0.430	−0.487	**1**

Values in bold are different from 0 with a significance level $a = 0.05$; T_{St} is the stability temperature.

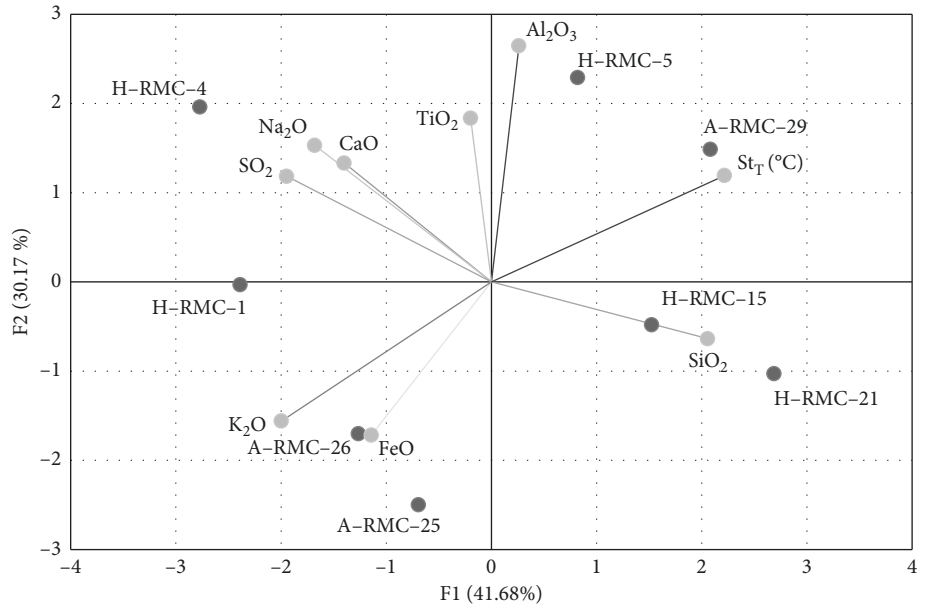

Figure 8: Principal component analyses of kaolin from Huayacocotla Ver. and Alumbres Hgo.

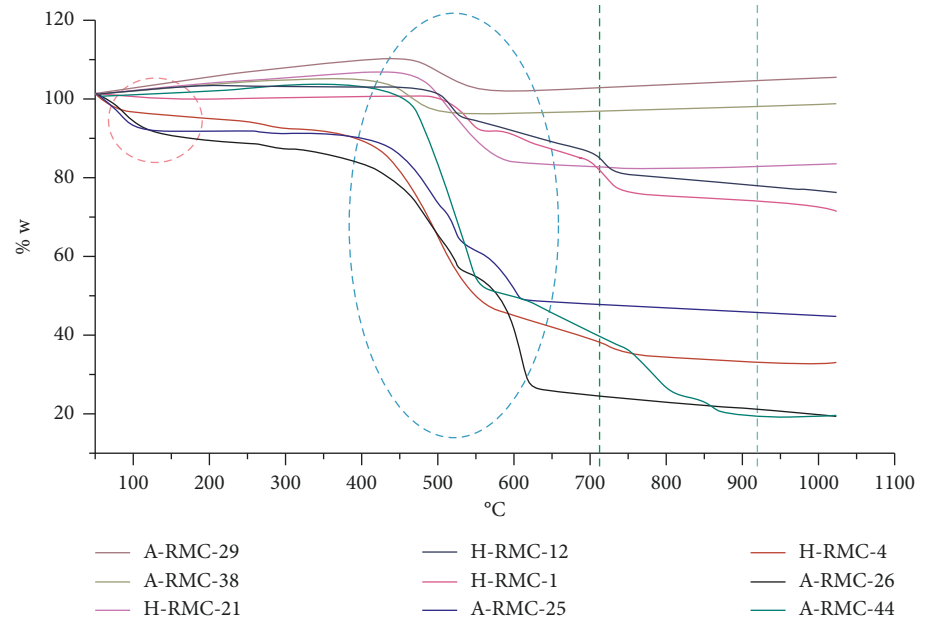

Figure 9: Thermograms of the kaolin samples from Huayacocotla, Ver., and Alumbres, Hgo.

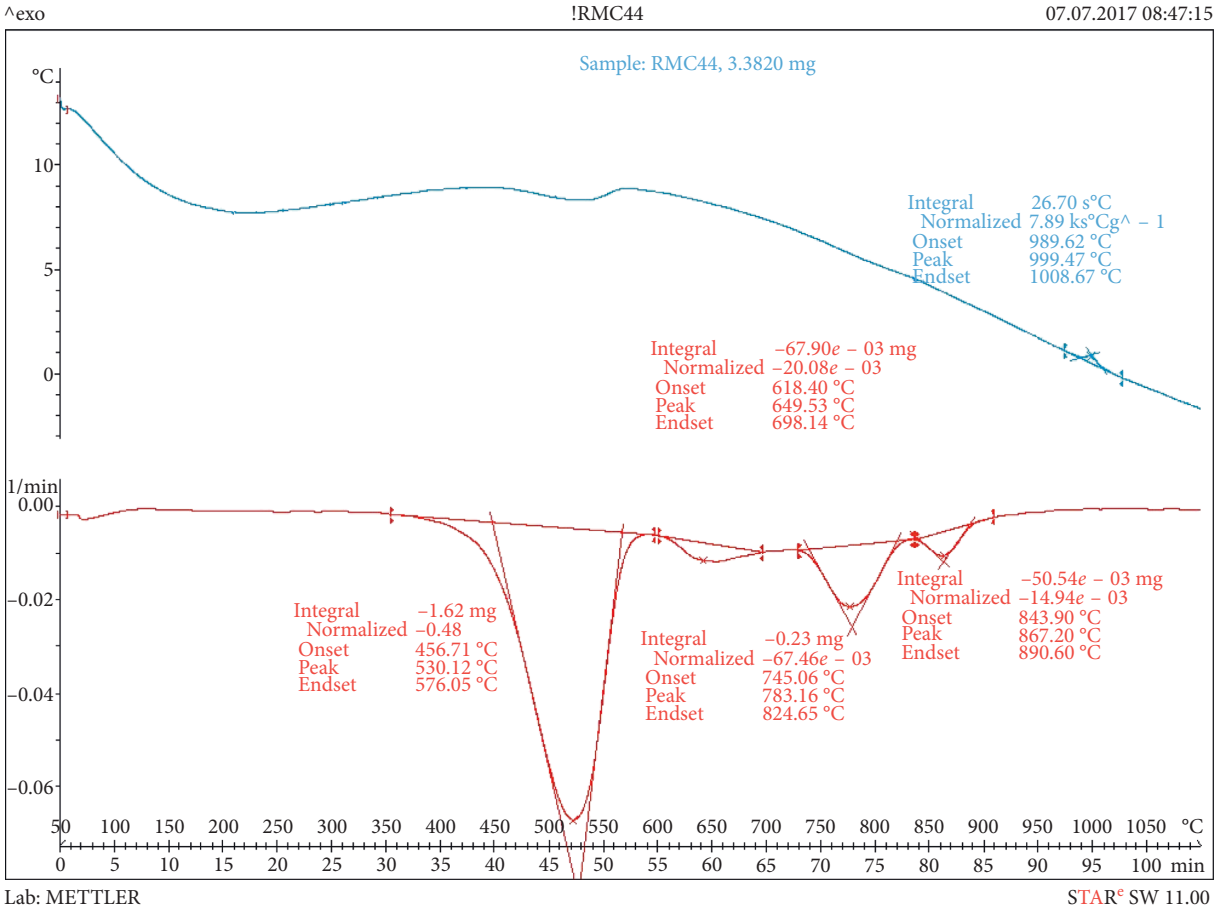

Figure 10: Thermogram for the A-RMC 44 sample from Alumbres, Hgo. Working condition: thermogravimetric analyzer, Mettler Toledo, Mod. TGA/SDTA851^e, range from 50°C up to 1100°C with a heating rate of 10°C min^{-1}, N_2 atmosphere, flow rate of 100 ml·min^{-1}.

principal mineral phases identified in the Alumbres samples are quartz and cristobalite. The secondary mineral phases detected in the Huayacocotla samples were kaolinite and quartz, and the secondary mineral phase detected in the Alumbres samples was dickite.

The kaolin alteration grade is different in the two areas; in Huayacocotla, there is hydrothermal alteration with the presence of primary minerals, such as plagioclase, feldspar, and quartz. In Alumbres, there is variation of clays and the presence of pyrite ores.

Finally, the trace mineral phases that have been determined in some samples are pyrite and sphalerite due to the calco-alkaline character of the argillic rock (kaolin), which has strong alteration accompanied by silicification.

The presence of mineral phases based on silica is due to the nature of the hosting rock, which comprises massive rhyolite and ignimbrite with some horizons of the rhyolitic domain. Therefore, the oxides and hydroxides with a greater presence in the kaolin samples are hematite (Fe_2O_3), limonite ($FeO(OH)\cdot nH_2O$), and goethite ($FeO(OH)$) due to the late hydrothermal formation associated with meteoric leaching.

The crystalline morphology is similar for the subhedral type in both zones; this allowed us to identify the presence of kaolinite and dickite in Huayacocotla and illite and kaolinite in Alumbres.

The kaolin thermal stability is approximately 1300°C, and it rises up to 1600°C with increases of the Al_2O_3 content. When the SiO_2 content increases, the thermal stability of kaolin decreases, and its vitrifying temperature is lower than the stability temperature. The presence of K_2O, Na_2O, CaO, and SO_2 reduces kaolin's stability temperature to the softening temperature of the material.

Kaolin that tolerated temperatures between 1300°C and 1600°C can be used as a coating for low-temperature furnaces, while that which presented a refractory character of the silico-aluminous type due to the content of SiO_2 (70–90%) and Al_2O_3 (10–30%) can be used as a high-temperature refractory material since it shows a softening temperature and stability up to 1600°C.

A structural formula estimation of the minerals was not possible due to the high content of secondary and tertiary minerals.

Data Availability

The data in Tables 1 and 2 were obtained from elemental analysis with support of calibrations standard curves, and

references included also support the finding of this study. Data supporting this research article are available from the corresponding author via e-mail.

Conflicts of Interest

The authors declare that they have no conflicts of interest.

Acknowledgments

The authors are grateful to CONACYT, PRODEP, and Autonomous University of the State of Hidalgo for the financial support and facilities provided to support this work.

References

[1] G.-I. Ekosse, "Kaolin deposits and occurrences in Africa: geology, mineralogy and utilization," *Applied Clay Science*, vol. 50, no. 2, pp. 212–236, 2010.

[2] M. Garcia-Valles, T. Pi, P. Alfonso et al., "Mineralogical and thermal characterization," *Clay Minerals*, vol. 50, no. 3, pp. 405–416, 2015.

[3] D. Gardner, *A Study of Mineral Impurities within the Georgia Kaolins*, Georgia State University, Atlanta, Georgia, USA, 2016.

[4] M. Jordan, M. Montero, S. Meseguer, and T. Sanfeliu, "Influence of firing temperature and mineralogical composition on bending strength and porosity of ceramic tile bodies," *Applied Clay Science*, vol. 42, no. 1-2, pp. 259–265, 2008.

[5] K. Singh, S. Kaur, H. Kaur, and K. Kaur, "Multifaceted role of clay minerals in pharmaceuticals," *Future Science OA*, vol. 1, no. 3, pp. 1–9, 2015.

[6] M. Valásková, "Clays, clay minerals and cordierite ceramics: a review," *Ceramics-Silikáty*, pp. 331–340, 2015.

[7] H. P. Alves, J. B. Silva, L. F. Campos, S. M. Torres, R. P. Dutra, and D. A. Macedo, "Preparation of mullite based ceramics from clay–kaolin waste mixtures," *Ceramics International*, vol. 42, no. 16, pp. 19086–19090, 2016.

[8] A. K. Chakraborty, *Phase Transformation of Kaolinite Clay*, Springer, New Delhi, India, 2014.

[9] W. Gonçalves, V. Silva, R. Menezes, G. Neves, H. Lira, and L. Santana, "Microstructural, physical and mechanical behavior of pastes containing clays and alumina waste," *Applied Clay Science*, vol. 137, pp. 259–265, 2016.

[10] P. Schroeder and G. Erickson, "Kaolin: from anciente porcelains to nanocomposites," *Elements*, vol. 10, no. 3, pp. 177–182, 2014.

[11] J. Srodon, V. Drits, D. McCarty, J. Hsieh, and D. Eberl, "Quantitative X-ray diffraction analysis of clay-bearing rocks from random preparations," *Clays and Clay Minerals*, vol. 49, no. 6, pp. 514–528, 2001.

[12] C. L. Fernández, *NORMA Oficial Mexicana NOM-021-RECNAT-2000, Que establece las especificaciones de fertilidad, salinidad y clasificación de suelos. Estudios, muestreo y análisis. Diario Oficial*, 2002.

[13] EPA, *Method 3052 Microwave Assisted Acid Digestion of Silicious and Organically Based Matrices, EPA SW-846, Revision 3*, Environmental Protection Agency, Washington, DC, USA, 2004.

[14] E. Muller, M. Mesko, D. Moraes, M. Korn, and E. Flores, "Wet digestion using microwave heating," *Microwave-Assisted Sample Preparation for Trace Element Determination*, pp. 99–142, Elsevier, Rio de Janeiro, Brazil, 2014.

[15] J. Walsh and R. Howie, "An evaluation of the performance of an inductively coupled plasma source spectrometer from the determination of the major and trace constituents of silicate rocks and minerals," *Mineralogical Magazine*, vol. 43, no. 332, pp. 967–974, 1980.

[16] D. Murphy, *Fundamentals of Light Microscopy and Electronic Imaging*, Wiley, London, UK, 2001.

[17] E. Pirard, "Multispectral imaging of ore minerals in optical microscopy," *Mineral Magazine*, vol. 68, no. 2, pp. 323–333, 2004.

[18] ASTM C24-01, *Standardd Test Method for Pyrometric Cone Equivalent (PCE) of Fireclay and High Alumina Refractory Materials C24-01*, ASTM International, West Conshohocken, PA, USA, 2001.

[19] Microsoft, Recuperado, 2016, website@xlstat.com, https://www.xlstat.com/es/descargar.

[20] R. Gaines, H. Skinner, E. Foord, B. Mason, and A. Rosenzweig, *Dana's New Mineraalogy: The System of Mineralogy of James Dwight and Edward Salisbury*, John Wiley & Sons Inc, Somerset, NJ, USA, 1997.

[21] M. Albert, L. Ortega, R. Lunar, F. Martínez, and R. Piña, "Mineralogy of the hydrothermal alteration in the Námafjall geothermal field (Iceland)," *Revista de la Sociedad Española de Mineralogía*, vol. 1, no. 15, pp. 25-26, 2011.

[22] K. Liu and G. Thomas, "Time-temperature-transformation curves for kaolinite-alfa-alumina," *Journal of the American Ceramic Society*, vol. 77, no. 6, pp. 545–552, 1994.

[23] H. Rezaire, W. Rainforth, and W. Lee, "Mullite evolution in ceramics derived from kaolinite, kaolinite with added alfa-alumina and Sol-Gel precursors," *British Ceramic Transactions*, vol. 96, no. 5, pp. 181–187, 1997.

[24] J. Shackelford and R. Doremus, *Ceramic and Glasss Materials*, Springer, New York, NY, USA, 2008.

[25] E. Jhonson and S. Arshad, "Hydrothermally synthesized zeolites based on kaolinite: a review," *Applied Clay Science*, vol. 97-98, pp. 215–221, 2014.

[26] B. Sonuparlak, M. Sarikaya, and I. Askay, "Spinel phase formation during the 980°C, exothermic reaction in the Kaolinite-to Mullite reaction series," *Journal of the American Ceramic Society*, vol. 70, no. 11, pp. 837–842, 1987.

[27] D. J. Duval, S. H. Risbud, and J. F. Shackelford, "Mullite," *Ceramic and Glass Materials: Structure, Properties and Processing*, p. 202, Berlin, Germany, 2008.